VERSITA

Synthesis, characterization, DC-electrical conductivity and γ-ray effect on Ag^{1+}, Y^{3+} double doped nano lithium manganates ($LiMn_{2-2x}Ag_xY_xO_4$) for rechargeable batteries

MORSI M. ABOU-SEKKINA[1], FAWAZ A. SAAD[2], FOUAD G. EL-METWALY[1,3],
ABDALLA M. KHEDR[1,2*]

[1]Chemistry Department, Faculty of Science, Tanta University, Tanta, Egypt

[2]Chemistry Department, College of Applied Sciences, Umm Al-Qura University, Makkah, Saudi Arabia

[3]Chemistry Department, Faculty of Science, Jazan University, Jazan, Saudi Arabia

Pristine lithium manganate ($LiMn_2O_4$) and Ag^{1+}, Y^{3+} double doped nano lithium manganate [$LiMn_{2-2x}Ag_xY_xO_4$, (x = 0.025, 0.05)] spinels were synthesized *via* a coprecipitation method for rechargeable batteries applications. The synthesized $LiMn_{1.9}Ag_{0.05}Y_{0.05}O_4$ was exposed to different doses of γ-irradiation (10 and 30 kGy). The resulting spinel products were characterized by using thermogravimetric and differential thermal analysis (TG/DTA), X-ray diffraction (XRD), infrared (IR) spectroscopy, scanning electron microscopy (SEM), energy dispersive analysis of X-rays (EDAX), electronic (UV-Vis) and electron spin resonance (ESR) spectra. $LiMn_2O_4$ exhibited a discharge capacity of 124 mAhg^{-1} while $LiMn_{1.9}Ag_{0.05}Y_{0.05}O_4$ had discharge capacities of 129 and 137 mAhg^{-1} for non irradiated and γ-irradiated (30 kGy) samples, respectively. The effects of the dopant cations and γ-irradiation on the discharge capacity and DC-electrical conductivity of some synthesized spinels were studied.

Keywords: *nano lithium manganates; Ag^{1+}, Y^{3+} double doped; γ-ray effect*

1. Introduction

Nano lithium manganate spinel ($LiMn_2O_4$) is an attractive candidate used in the power sources of portable electronic devices (laptop computers, cell phones, etc.) to store electricity from renewable sources, and as a vital component in new hybrid electric vehicles, due to its high electromotive force and high energy density [1, 2]. Also, $LiMn_2O_4$ spinel is the best choice to be the positive electrode (cathode) of rechargeable lithium ion batteries due to its low cost, non-toxic nature, efficiency, environmental friendliness and ease of preparation when compared with other layered oxides used for rechargeable lithium ion batteries such as lithium cobalt oxide ($LiCoO_2$) and lithium nickel oxide ($LiNiO_2$) [3–5]. $LiCoO_2$ has many disadvantages such as high cost, toxicity, a nega-

tive environmental impact and a low practical specific capacity against its theoretical value. There are several research articles reporting that the capacity of pure spinel $LiMn_2O_4$ diminishes at high reduction levels [6, 7]. The capacity fading of lithiated transition metal oxides such as $LiCoO_2$, $LiNiO_2$ and $LiMn_2O_4$ occurs due to various factors such as Jahn-Teller distortion (change of a cubic symmetry into tetragonal one, a two-phase unstable reaction), slow dissolution of manganese into the electrolyte [8], lattice instability [9] and particle-size distribution [10, 11]. To suppress the Jahn-Teller distortion and obtain high cycling capacity, many researchers have studied Li–Mn–O spinels in order to improve cycleability by partially chemical substitution of Mn^{3+} with various divalent, trivalent and tetravalent-doped cations such as Sm, Co, Zn, Ca, Fe, Ni, Cd, Tb, Ga, Ti, Al, V and Cr [12–16]. Ohuzuku et al. [10] and Lee et al. [17] have reported that partial doping of divalent and trivalent

*E-mail: abkhedr2010@yahoo.com

cations is more effective in suppressing the capacity fade during cycling. The substitution increases the average oxidation state of Mn above 3.5, hence suppressing Jahn-Teller distortion, this leads to stabilizing the crystal structure of spinel. We reported here, the preparation of $LiMn_2O_4$ and Ag^{1+}, Y^{3+} double doped nano lithium manganese oxide [$LiMn_{2-2x}Ag_xY_xO_4$, (x = 0.025, 0.05)] spinels by using a coprecipitation method. The synthesized spinels were characterized by various techniques such as thermal analysis (TG/DTA), XRD, SEM, EDAX, IR, UV-Vis and ESR spectroscopy. The effects of dopant cations and γ-irradiation on the discharge capacity and DC-electrical conductivity of the prepared spinels were also investigated and discussed.

2. Experimental

2.1. Synthesis of nano spinels

Pure $LiMn_2O_4$ and double doped $LiMn_{2-2x}Ag_xY_xO_4$ (x = 0.025, 0.05) spinels were synthesized by coprecipitation method, where stoichiometric amounts of LiOH solution and oxalic acid solution were mixed with each other. The mixture was added to a hot solution of manganese acetate dropwise with stirring at 80 °C. Yellow white precipitate was obtained and vinegar odor was smelt. The obtained mixture was further heated with continuous stirring to remove the excess of acetic acid and water, and dried for 12 h to obtain the $LiMn_2C_2O_4(Ac)$ precursor. Then, it was mixed with cation-doped compounds, ground thoroughly and pre-sintered at 600 °C for 4 h. Then, they were ground and pressed into pellets, sintered in air at 850 °C for 8 h at a heating rate of 10 °C/min. After sintering, the samples were cooled with a possible lowest rate (5 °C/min).

2.2. Instruments and characterization

The thermal gravimetric analysis (TGA) was carried out in a dynamic nitrogen atmosphere (20 mL min^{-1}) with a heating rate of 10 °C min^{-1} using a Shimadzu TG-50 thermogravimetric analyzer. DTA of green samples (uncalcined) were recorded by a Du Pont Instruments 990 ther-

mal analyzer (England) with a heating rate of 10 °C min^{-1} at Central Laboratory, Tanta University. The crystal structure of the prepared samples was analyzed by a Phillips (Holland) X-ray diffractometer using Cu Kα radiation (λ = 1.54056 Å) operating at 40.0 kV, 30.0 mA and the data were collected in the $10 - 80°$ 2θ range. The infrared spectra were recorded using a Perkin-Elmer 1430 IR spectrophotometer within the range of 1000 to 200 cm^{-1} for all samples in a form of KBr discs. The morphology of the prepared samples was investigated by scanning electron microscopy (SEM, JSM-5300LV, Japan) and the dispersion of Ag was visualized by energy dispersive analysis of X-rays (EDAX). The electronic absorption spectra were recorded using a Shimadzu UV-Vis 160A spectrophotometer from 200 to 800 nm using Nujol mull technique. Room temperature x-band powder electron spin resonance spectra were recorded using a Jeol spectrometer model JES-FE2XG equipped with an E101 microwave bridge using DPPH as a reference. Some samples were exposed to different doses of γ-irradiation (10 and 30 KGy) with the dose rate of 3.52 KGy/h by Indian gamma rays source at National Center for Radiation Research and Technology, Nasr City, Cairo, Egypt. DC-electrical conductivity of the synthesized samples sintered at 850 °C for 8 h was recorded using the two terminal DC-electrical conductivity method, where the pellets of the samples were coated with silver paste, inserted between the two copper probes of the circuit using a Akeithly 175 multimeter (USA). This was done at the temperature range from room temperature up to 370 °C. The temperature was measured by a calibrated chromel-alumel thermocouple placed firmly at the sample during measurements.

2.3. Electrochemical studies

Cathode specimens were prepared by mixing the Li–Mn–O spinel powder with 10 wt.% acetylene black and 5 wt.% polyvinylidene fluoride (PVDF) in n-methyl pyrrolidone (NMP) solution. Electrodes were dried under vacuum at 110 °C for at least 2 h before use. Lithium foil was used as reference and counter electrodes. The electrolyte

contained l M LiPF$_6$ in ethylene carbonate/diethyl carbonate (EC:DEC = 1:1). The cell assembly was put into a dry box under argon atmosphere.

3. Results and discussion

3.1. Thermal studies

Fig. 1 shows the TGA-DTA curves of the precursor that was fired to give LiMn$_{2-2X}$Ag$_X$Y$_X$O$_4$ nano spinel. There are three weight-loss regions on the curves. The first region, from room temperature to 100 °C, may be attributed to the removal of bonded and absorbed water, corresponding to weak endothermic peak at 57 °C in the DTA curve. In the second region of weight loss, from 120 to 160 °C, one sharp exothermic reaction peak at 160 °C is considered to be due to the departure of methyl group, for which weight loss is noticeable. In the third region, the weight loss of 39 % is attributed to combustion of residual organic constituents and loss of excess oxygen in the range of 215 to 450 °C (corresponding to medium broad endothermic peak at 350 °C in DTA curve), and then the LiMn$_2$O$_4$ phase is formed. In the region from 450 to 900 °C, the TGA curve becomes flat and no sharp peaks can be observed in the DTA curve, indicating that no phase transformation occurs.

3.2. X-ray diffraction studies

X-ray powder diffraction (XRD) patterns of the pure and double doped spinels with different content of Ag^{1+}, Y^{3+} are shown in Fig. 2. All diffraction peaks are very strong which reveals that the samples have good cubic crystal structures. These structures correspond to cubic stander spinel LiMn$_2$O$_4$ with the space group Fd3m (JCPDS Cards-No. 35-0782), JCPDS (Joint Committee on Power Diffraction Standard). They are made up of a regular tetrahedron LiO$_4$ and octahedron MnO$_6$ [18]. The lattice constant and crystal volume of Ag^{1+},Y^{3+} doped spinel (Table 1) are smaller than the undoped one and increase with increasing dopant content since the radius of the sixth coordination Ag^{1+} (1.15 Å), Y^{3+} (0.90 Å) is bigger than the one of Mn^{3+} (0.66 Å). XRD of γ-irradiation samples with 10, 30 kGy are shown

in Fig. 3. Also, all diffraction peaks of γ-irradiated samples are very strong indicating that the samples have a good cubic crystal structure but the peaks have small shifts to lower angles. These small shifts indicate high stability of the doped spinels against ultra-high energy γ-rays.
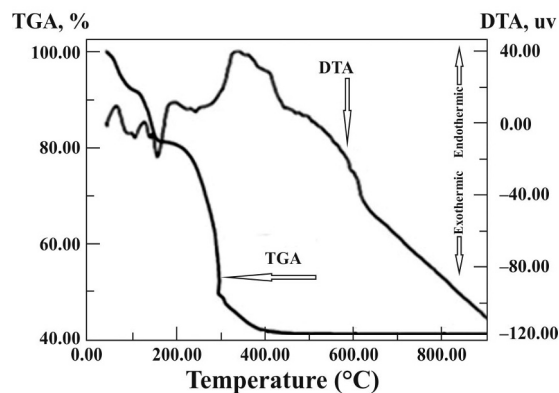
Fig. 1. TGA/DTA curves for LiMnC$_2$O$_4$(Ac) precursor containing Ag^{1+} and Y^{3+} dopants.
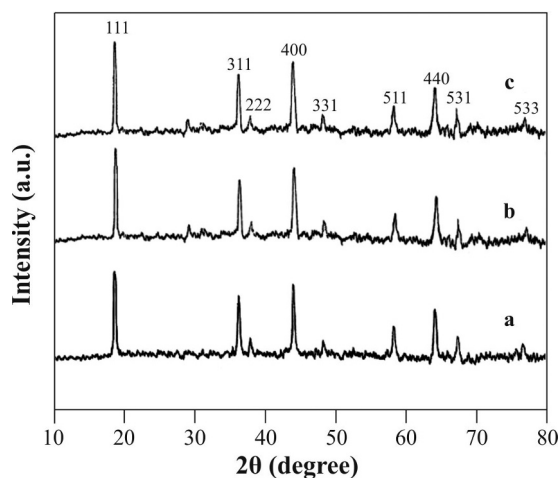
Fig. 2. X-ray diffraction patterns of undoped and doped nano Li–Mn–O spinels (LiMn$_{2-2x}$Ag$_x$Y$_x$O$_4$): (a) undoped LiMn$_2$O$_4$, (b) LiMn$_{1.95}$Ag$_{0.025}$Y$_{0.025}$O$_4$ and (c) LiMn$_{1.9}$Ag$_{0.05}$Y$_{0.05}$O$_4$.

3.3. IR spectral studies

Vibrational modes attributed to the motion of cations with respect to their oxygen neighbors are sensitive to the point group symmetry

Table 1. Lattice constants and unit cell volumes of $LiMn_2O_4$, $LiMn_{1.95}Ag_{0.025}Y_{0.025}O_4$ and $LiMn_{1.9}Ag_{0.05}Y_{0.05}O_4$ spinels.

No	Sample		Lattice constants, a (Å)	Unit cell volume (Å^3)
1	$LiMn_2O_4$		8.186	549
2	$LiMn_{1.95}Ag_{0.025}Y_{0.025}O_4$		8.228	557
3	$LiMn_{1.9}Ag_{0.05}Y_{0.05}O_4$		8.327	577
4	$LiMn_{1.9}Ag_{0.05}Y_{0.05}O_4$	γ-irradiated with 10 kGy	8.300	572
5	$LiMn_{1.9}Ag_{0.05}Y_{0.05}O_4$	γ-irradiated with 30 kGy	8.279	568
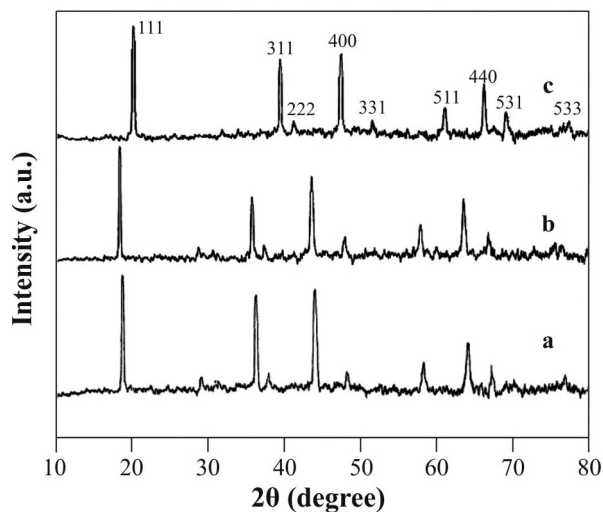
Fig. 3. X-ray diffraction patterns of non irradiated and γ-irradiated $LiMn_{1.9}Ag_{0.05}Y_{0.05}O_4$ nano spinels: (a) non irradiated $LiMn_{1.9}Ag_{0.05}Y_{0.05}O_4$ spinel, (b) $LiMn_{1.9}Ag_{0.05}Y_{0.05}O_4$ spinel γ-irradiated with 10 kGy and (c) $LiMn_{1.9}Ag_{0.05}Y_{0.05}O_4$ spinel γ-irradiated with 30 kGy.

of the cations in the oxygen host matrix [19]. Hence, the local environment of the cations in a lattice of close-packed oxygen can be studied by IR spectroscopy [20]. Infrared spectra of pure nano $LiMn_2O_4$, $LiMn_{1.95}Ag_{0.025}Y_{0.025}O_4$, and $LiMn_{1.9}Ag_{0.05}Y_{0.05}O_4$ spinels sintered at 850 °C for 8 h are shown in Fig. 4. In the spectra of pure nano $LiMn_2O_4$, the observed high-frequency bands, located around 618 and 517 cm^{-1}, are associated with the asymmetric stretching modes of MnO_6 octahedron whereas the band at 260 cm^{-1} is attributable to mixed characters: octahedral MnO_6

and tetrahedral LiO_4 building the cubic lattice of nano $LiMn_2O_4$.
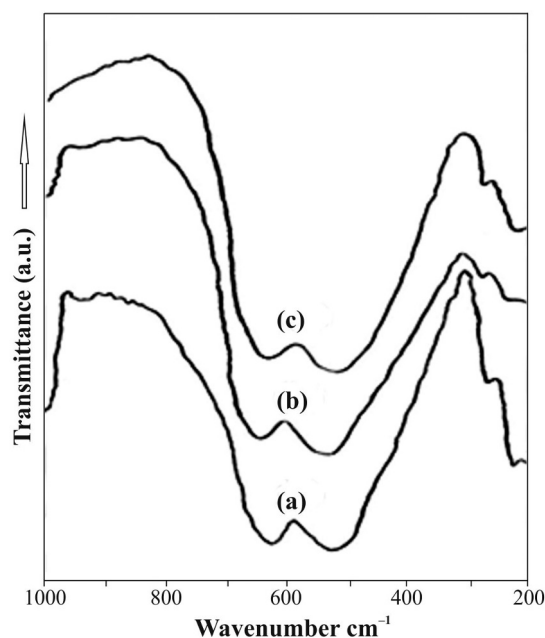
Fig. 4. IR spectra of undoped and doped Li–Mn–O spinels ($LiMn_{2-2X}Ag_XY_XO_4$) fired at 850 °C in air for 8 h: (a) undoped $LiMn_2O_4$ spinel, (b) $LiMn_{1.95}Ag_{0.025}Y_{0.025}O_4$, and (c) $LiMn_{1.9}Ag_{0.05}Y_{0.05}O_4$.

These results are quite similar to those given in earlier reports [21, 22]. It can also be seen from Fig. 4 that the vibration frequency of two stretching modes in the MnO_6 group reveals small changes with increasing the dopant contents. For double doped Ag^{1+}, Y^{3+} nano spinel, the peaks shifted from 517 to 514 and from 618 to 616 cm^{-1} for x = 0.025 whereas the peaks shifted from 517 to
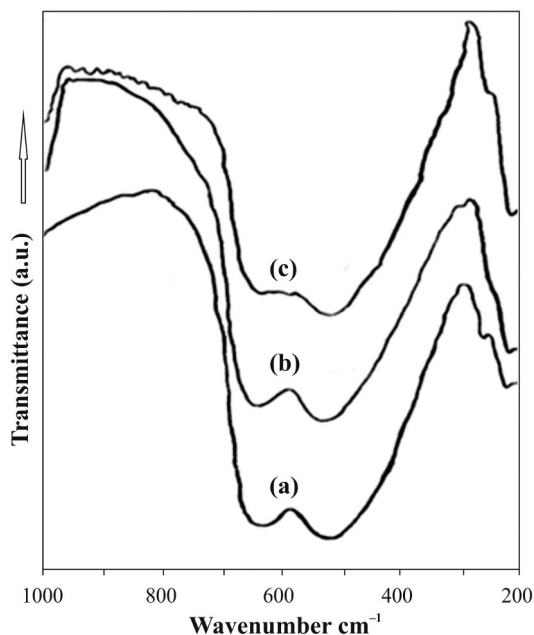
Fig. 5. IR spectra of non irradiated and γ-irradiated LiMn$_{1.9}$Ag$_{0.05}$Y$_{0.05}$O$_4$ spinels: (a) non irradiated LiMn$_{1.9}$Ag$_{0.05}$Y$_{0.05}$O$_4$ spinel, (b) LiMn$_{1.9}$Ag$_{0.05}$Y$_{0.05}$O$_4$ spinel irradiated with 10 kGy and (c) LiMn$_{1.9}$Ag$_{0.05}$Y$_{0.05}$O$_4$ spinel irradiated with 30 kGy.

509 and 618 to 625 cm^{-1} for x = 0.050. This is good evidence to the insertion of Ag^{1+}, Y^{3+} in octahedral position. IR spectra of non irradiated LiMn$_{1.9}$Ag$_{0.05}$Y$_{0.05}$O$_4$ and those γ-irradiated with 10, 30 kGy (Fig. 5) indicate that the samples are still nano cubic spinel but there are shifts of peaks from 509, 625 cm^{-1} before irradiation to 512, 626 cm^{-1} and 512, 627 cm^{-1} after γ-irradiation with 10, 30 kGy, respectively.

3.4. SEM and EDAX analysis

The morphology of pure and doped samples was investigated by scanning electron microscope (SEM) after coating with gold. Fig. 6 shows the observed images for pure LiMn$_2$O$_4$, double doped LiMn$_{1.95}$Ag$_{0.025}$Y$_{0.025}$O$_4$, LiMn$_{1.9}$Ag$_{0.05}$Y$_{0.05}$O$_4$ and γ-irradiated double doped LiMn$_{1.9}$Ag$_{0.05}$Y$_{0.05}$O$_4$. The images reveal that the powder exhibits nano crystals in agreement with the data obtained from X-ray studies. These images denote irregular porous morphology, this porous morphology is beneficial for the diffusion of electrolyte into the interior of the particle during fabrication of the spinels.
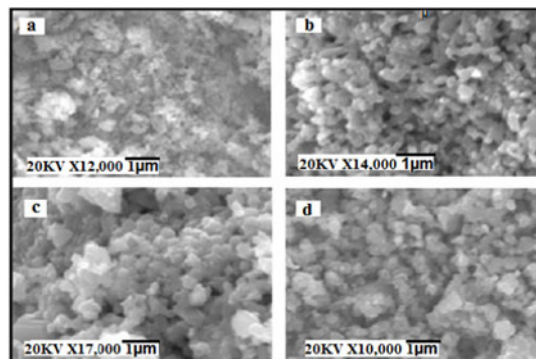
Fig. 6. SEM images of LiMn$_{2-2X}$Ag$_X$Y$_X$O$_4$ spinels: (a) LiMn$_2$O$_4$, (b) LiMn$_{1.95}$Ag$_{0.025}$Y$_{0.025}$O$_4$, (c) LiMn$_{1.9}$Ag$_{0.05}$Y$_{0.05}$O$_4$ and (d) LiMn$_{1.9}$Ag$_{0.05}$Y$_{0.05}$O$_4$ spinel irradiated with 30 kGy.
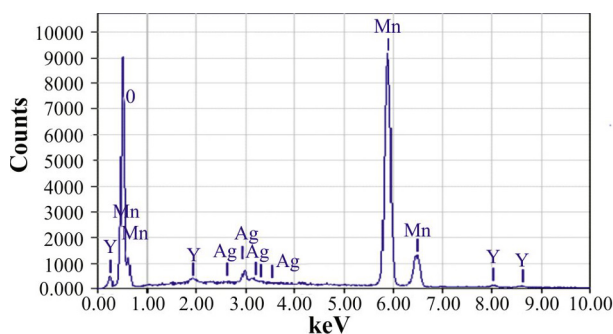
Fig. 7. EDAX profile of nano LiMn$_{1.9}$Ag$_{0.05}$Y$_{0.05}$O$_4$ spinel.

Fig. 7 represents EDAX profiles of nano LiMn$_{1.9}$Ag$_{0.05}$Y$_{0.05}$O$_4$ spinel. These profiles of the reflections corresponding to the constituent elements of prepared sample agree with that published by Helan et al. [23], Xiong et al. [24] and Thirunakaran et al. [25, 26].

3.5. ESR and UV-Vis spectra

The paramagnetic behavior of the synthesized crystals was investigated using ESR spectroscopy. Fig. 8 shows the ESR spectrum of the LiMn$_{1.9}$Ag$_{0.05}$Y$_{0.05}$O$_4$ nano compound. The spectrum displays ESR signal attributed to Mn^{3+} ions

centered at 3380 G and the corresponding value of g factor is 1.992, which is in good agreement with the reported value for $LiMn_2O_4$.

The UV-Vis spectra of pure nano $LiMn_2O_4$ spinel display a strong absorption peak at 237 nm, medium peak at 341 nm and weak peak at 380 due to d-d transitions in manganese ion. The double doped $LiMn_{1.9}Ag_{0.05}Y_{0.05}O_4$ nono spinel shows two weak peaks at 272, 300 nm and strong one at 342 nm assigned to d-d transitions in Mn^{3+}, Ag^{1+} and Y^{3+}.
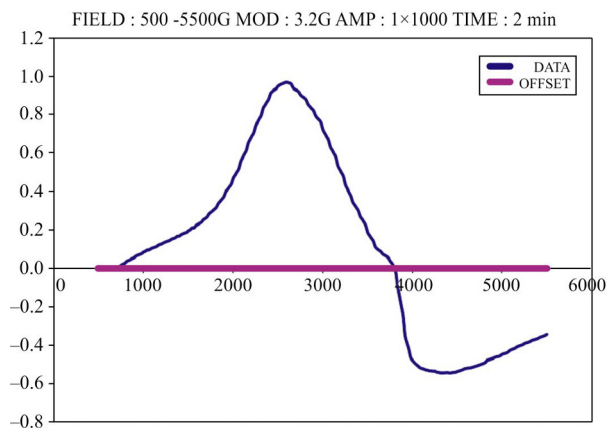
Fig. 8. ESR spectrum of nano $LiMn_{1.9}Ag_{0.05}Y_{0.05}O_4$ spinel.

3.6. Electrochemical studies

Fig. 9 – 11 show charge-discharge curves of $LiMn_2O_4$, non irradiated $LiMn_{1.9}Ag_{0.05}Y_{0.05}O_4$ and γ-irradiated $LiMn_{1.9}Ag_{0.05}Y_{0.05}O_4$ (30 kGy). All curves show two plateaus that are good indication for de-intercalation/intercalation of Li^{1+} ions at the 8a tetrahedral sites. $LiMn_2O_4$ delivers a discharge capacity of 124 $mAhg^{-1}$ and non-irradiated $LiMn_{1.9}Ag_{0.05}Y_{0.05}O_4$ delivers a discharge capacity of 129 $mAhg^{-1}$ whereas $LiMn_{1.9}Ag_{0.05}Y_{0.05}O_4$ γ-irradiated with 30 kGy delivers a discharge capacity of 137 $mAhg^{-1}$. The open-circuit energy diagram of a lithium battery has been discussed by Goodenough et al. [27, 28]. If the active transition-metal cation contains a localized d-electron manifold, the manifold acts as a redox couple, e.g. $Ni^{2+/4+}$ in $LiNi_{1.5}Mn_{0.5}O_4$. Successive redox couples are separated by an on-site

effective Coulomb correlation energy U that can be large when augmented by either a crystal-field splitting or an intra-atomic exchange splitting [29].
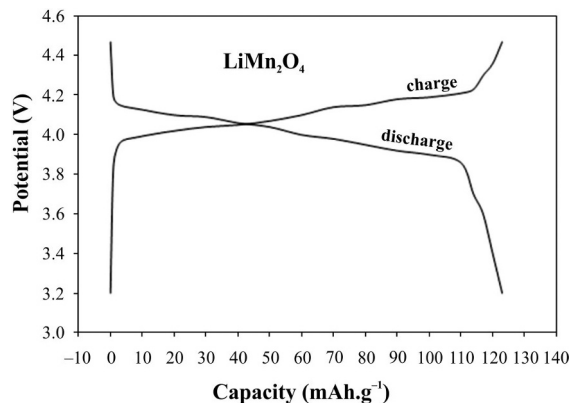
Fig. 9. Charge-discharge curves of pure $LiMn_2O_4$ spinel.
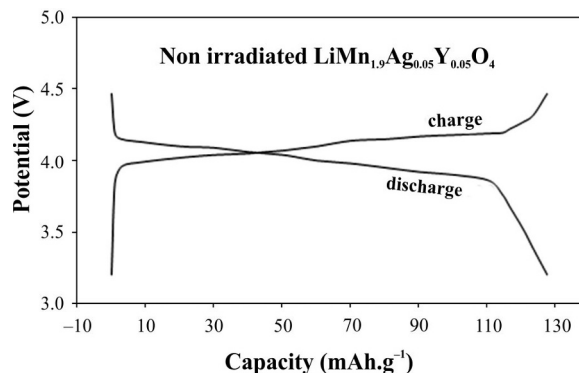
Fig. 10. Charge-discharge curves of non-irradiated $LiMn_{1.9}Ag_{0.05}Y_{0.05}O_4$ calcined at 850 °C.

However, when the Fermi energy (*EFC*) of the cathode material approaches the top of the anion p bands of the host, the p-d covalent mixing may transform the correlated d electrons at *EFC* into band electrons occupying one-electron states [27, 30]. In the absence of a crystal-field splitting of the d orbitals at *EFC*, which is the case for Ni(IV) to Ni(II), the one-electron states are not separated by any on-site energy U and there is no step in the voltage of the battery. *EFC* is moved from one formal valence state to another upon the reduction or oxidation of the host. This confirms
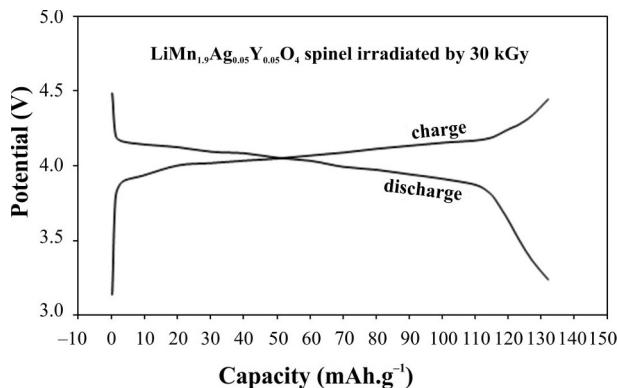
Fig. 11. Charge-discharge curves of LiMn$_{1.9}$Ag$_{0.05}$Y$_{0.05}$O$_4$ spinel irradiated with 30 kGy.

that substituted Ag^{1+} and Y^{3+} ions take part in the topotactic redox reaction during charge/discharge process of the cell [31].

Substitution of 2.5 and 5 % Ag and Y for Mn in LiMn$_2$O$_4$ spinel has been chosen because this composition implies that Mn is in the 4+ valence, thus avoiding the Jahn-Teller (JT) distortion associated to Mn^{3+}. Also, the partial replacement of Mn by Ag and Y in LiMn$_{2-2X}$Ag$_X$Y$_X$O$_4$ is an effective way to alleviate the problem of oxygen loss generating Mn^{3+} ions in LiMn$_2$O$_4$ framework. Thus, it can be demonstrated that the Ag and Y-doping stabilizes the lattice without impacting the capacity significantly, but it decreases the energy density [31, 32].

3.7. DC-electrical conductivity measurements

No references have been found in the literature concerning the studies on the electrical DC or AC conductivity of undoped and doped LiMn$_2$O$_4$ in the range of temperature from room temperature up to 370 °C. According to the Arrhenius equation [33]: $\sigma = \sigma°\mathrm{e}^{-\Delta Ea/kBT}$, where σ is the electrical conductivity at absolute temperature T, $\sigma°$ is the maximum electrical conductivity (that it would have at infinite temperature), k$_B$ is Boltzmann's constant = 8.61x10^{-5} eV K^{-1}, and ΔE$_a$ is the activation energy for electrical conduction, which indicates the energy needed for an ion to jump to a free hole. The conduction in LiMn$_2$O$_4$ nano spinel occurring via small-polaron hopping between Mn^{3+}

and Mn^{4+}, i.e. unpaired electrons from the e$_g$ orbitals of high-spin Mn^{3+} (d$_4$) hop to neighboring low-spin Mn^{4+} (d$_3$) ions. Both the e$_g$ orbitals of metal ion lie on the same octahedral site. So, they are equivalent in energy. Fig. 12 represents the variation of DC-electrical conductivity (lnσ) of pure non irradiated and irradiated LiMn$_2$O$_4$ spinels versus 1000/T. There is a positive temperature coefficient of electrical conductivity dσ/dT in the range of 20 to 370 °C which means that LiMn$_2$O$_4$ is a semiconductor in this range, with the activation energy of 0.312 eV. The activation energy reduces with irradiation with γ-ray (30 kGy) to 0.264 eV. Fig. 13 shows the variation of DC-electrical conductivity versus 1000/T for non-irradiated and irradiated LiMn$_{2-2X}$Ag$_X$Y$_X$O$_4$ nano spinels. These samples behaved as extrinsic semiconductor in the range of 20 to 370 °C with activation energies equal 0.351 and 0.380 eV for LiMn$_{1.95}$Ag$_{0.025}$Y$_{0.05}$O$_4$ and LiMn$_{1.9}$Ag$_{0.05}$Y$_{0.05}$O$_4$.
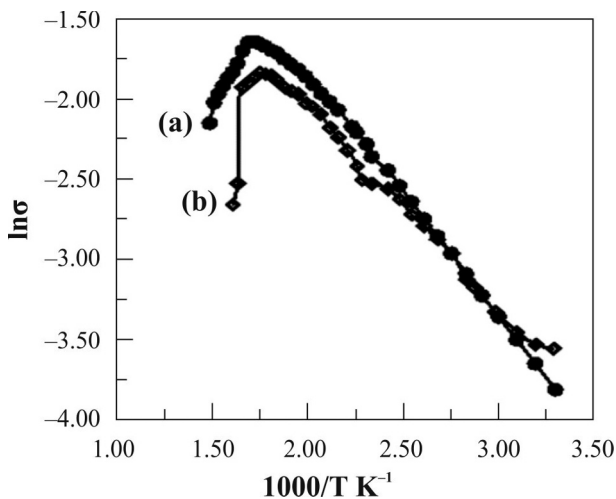
Fig. 12. The variation of DC-electrical conductivity (lnσ) versus reciprocal of absolute temperature (1000/T K^{-1}) for LiMn$_2$O$_4$ nanospinels: (a) non-irradiated sample and (b) sample irradiated with 30 kGy of γ-irradiation.

Upon γ-irradiation of LiMn$_{1.9}$Ag$_{0.05}$Y$_{0.05}$O$_4$ with 10 and 30 kGy, the activation energies decrease to 0.353 and 0.326 eV, respectively. This means that the activation energies are affected by increasing the dopant content and irradiation dose. In our future studies, it would be interesting to
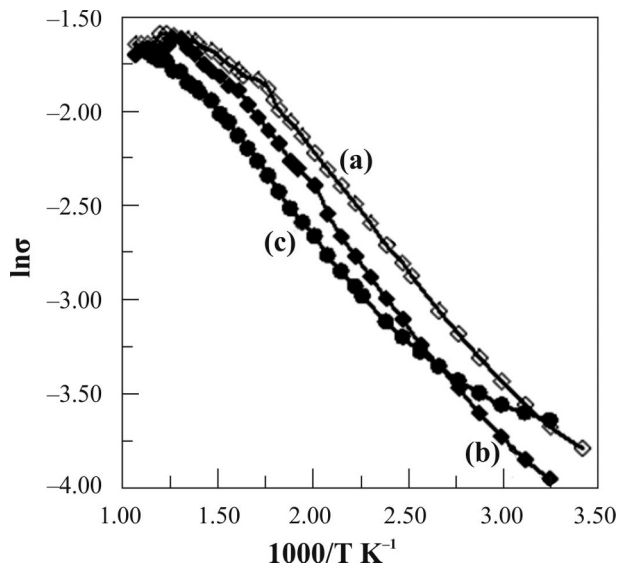
Fig. 13. The variation of DC-electrical conductivity ($\ln\sigma$) versus reciprocal of absolute temperature ($1000/T$ K^{-1}) for $LiMn_{1.95}Ag_{0.025}Y_{0.025}O_4$ (a), $LiMn_{1.9}Ag_{0.05}Y_{0.05}O_4$ (b) and $LiMn_{1.9}Ag_{0.05}Y_{0.05}O_4$ γ-irradiated with 10 kGy (c).

show how the obtained electrical conductivity corresponds with the electrochemical tests.

4. Conclusions

Pure $LiMn_2O_4$ and Ag^{1+}, Y^{3+} double doped lithium manganese oxide [$LiMn_{2-2x}Ag_xY_xO_4$ ($x = 0.25$, 0.05)] spinels were synthesized by a simple coprecipitation method and some of the prepared spinels were subjected to γ-irradiation. X-ray diffraction data revealed the formation of single-phase spinel with cubic crystal structure for pure and doped samples. X-ray diffraction calculation and SEM images indicated that the prepared spinels were nano compounds with porous morphology. The electrochemical studies denoted that incorporation of Ag^{1+} and Y^{3+} ions into $LiMn_2O_4$ effectively improves the stability and discharge capacity of pristine $LiMn_2O_4$, which are significant requirements for practical application of $LiMn_2O_4$-based lithium-ion batteries. The method used for preparation has a great potential for the commercial preparation of pure and doped $LiMn_2O_4$ spinels.

References

[1] TARASCON J.M., ARMAND M., *Nature*, 414 (2001), 359.

[2] GOUA D., CHANGA Z., TANGA H., LIA B., XUA X., YUANB X., WANGB H., *Electrochim. Acta*, 123 (2014), 254.

[3] TARASCON J.M., MCKINNON W.R., COOWAR F., BOWNER T.N., AMATUCCI G., GUYOMARD D.J., *J. Electrochem. Soc.*, 141 (1994), 1431.

[4] GUMMOW R.J., KOCK DE A., THACKERAY M.M., *Solid State Ionics*, 69 (1994), 67.

[5] THACKERAY M.M., KOCK DE A., ROSSOUW M.H., LILES D., BITTIHN R., HOGE D., *J. Electrochem. Soc.*, 139 (1992), 366.

[6] XIA Y., YOSHIO M., *J. Electrochem. Soc.*, 144 (1997), 2600.

[7] PISTOIA G., ANTONINI A., ROSATI R., ZANE D., *Electrochim. Acta*, 41 (1996), 2689.

[8] JANG D.H., SHIN J., OH S.M., *J. Electrochem. Soc.*, 143 (1996), 2211.

[9] YAMADA A., *J. Solid State Chem.*, 122 (1996), 165.

[10] OHUZUKU T., TAKEDA S., IWANAGA M., *J. Power Sources*, 90 (1999), 82.

[11] SONG D., IKUTA H., UCHIDA T., WAKIHARA M., *Solid State Ionics*, 117 (1999), 156.

[12] KHEDR A.M., ABOU-SEKKINA M.M., EL-METWALY F.G., *J. Electron. Mater.*, 42 (2013), 1275.

[13] JAVEDIQBAL M., ZAHOOR S., *J. Power Sources*, 165 (2007), 397.

[14] ABOU-SEKKINA M.M., KHEDR A.M., EL-METWALY F.G., *Chem. Mater. Res.*, 3 (2013), 15.

[15] KUMAR G., SCHLORB H. AND RAHNER D., *Mater. Chem. Phys.*, 70 (2001), 123.

[16] SAAD F.A., ABOU-SEKKINA M.M., KHEDR A.M., EL-METWALY F.G., *Int. J. Electrochem. Sc.*, 9 (2014), 3904.

[17] LEE J.H., HONG J.K., JANG D.H., SUN Y.K., OH S.M., *J. Power Sources*, 89 (2000), 714.

[18] TU J., ZHAO X.B., CAO G.S., TU J.P., ZHU T.J., *Mater. Lett.*, 59 (2005), 2886.

[19] ROUGIER C.J., NAZRI G.A., JULIEN C., *Mater. Res. Soc. Symp. Proc.*, 453 (1997), 647.

[20] ROUGIER C.J., NAZRI G.A., JULIEN C., *Ionics*, 3 (1997), 170.

[21] RICHARDSON T.J., ROSS P.N., *Mater. Res. Bull.*, 31 (1996), 935.

[22] CHITRA S., KALYANI P., MOHAN T., MASSOT M., ZIOLKIEWICZ S., GANGADHARAN R., EDDRIEF M., JULIEN C., *Ionics*, 4 (1998), 1.

[23] HELAN M., BERCHMAN L., JOSE T., VISUVASAM A., ANGAPPAN S., *Mater. Chem. Phys.*, 124 (2010), 439.

[24] XIONG L., XU Y., TAO T., GOODENOUGH J.B., *J. Power Sources*, 199 (2012), 214.

[25] THIRUNAKARAN R., SIVASHANMUGAM A., GOPUKUMAR S., RAJALAKSHMI R., *J. Power Sources*, 187 (2009), 565.

[26] THIRUNAKARAN R., RAVIKUMAR R., GOPUKUMAR S., SIVASHANMUGAM A., *J. Alloy Comp.*, 556 (2013), 266.

[27] GOODENOUGH J.B., KIM Y., *Chem. Mater.*, 22 (2010), 587.

[28] LIU D., HAN J., DONTIGNY M., CHAREST P., GUERFI A., ZAGHIB K., GOODENOUGH J.B., *J. Electrochem. Soc.*, 157 (2010), 770.

[29] GOODENOUGH J.B., *Oxides cathodes. In Advances in Lithium-Ion Batteries*, Kluwer Academic/Plenum, New York, 2002.

[30] MANTHIRAM A., *Chemical and Structural Stabilities of Layered Oxide Cathodes. In New Trends in Intercalation Compounds for Energy Storage*, NATO Science Series, Kluwer Academic Publishers, Dordrecht, 2002.

[31] JULIEN C.M., MAUGER A., ZAGHIB K., GROULT H., *Inorganics*, 2 (2014), 132.

[32] LIU D., HAMEL-PAQUET J., TROTTIER J., BARRAY F., GARIEPY V., HOVINGTON P., GUERFI A., MAUGER A., JULIEN C.M., GOODENOUGH J.B., *J. Power Sources*, 217 (2012), 400.

[33] RAMAN R., MURTHY V.R.K., VISWANATHAN B., *J. Appl. Phys.*, 69 (1991), 4053.